Physica Scripta. Vol. 68, C82–89, 2003

Photoassociation of Ultracold Sodium Atoms

A. Amelink and P. van der Straten

Debye Institute, Department of Atomic and Interface Physics, Utrecht University, P.O. Box 80,000, 3508 TA Utrecht, The Netherlands

Received September 2, 2000; revised version received March 15, 2001; accepted April 10, 2001

PACS ref: 33.20.–t, 34.50.Gb

Abstract

Using ultra-cold atoms a new technique of photoassociation spectroscopy has been developed. The technique has an unprecedented resolution and can be used to obtain high-resolution data on singly and doubly excited states of diatomic molecules. We describe the principle of the technique and show results for one specific case, namely the Na_2 molecule.

I. Introduction

The invention of methods for the laser cooling of atoms has opened the pathway for the study of ultracold collisions. Laser cooling techniques have been developed two decades ago with the principal idea, that cold atoms provide the ideal medium for high resolution spectroscopy due to the suppression of Doppler effects. Using laser cooling and trapping atoms could be brought to nearly complete stand still and be monitored during a long interaction time. However, soon it became apparent that the lifetime of cold atoms in the trap is limited by the collisions either with atoms in the background gas or by collisions with atoms in the trap. These processes as the main loss channel of atoms from the trap were subsequently studied in detail and pointed at the fact, that trap losses were severely enhanced by the use of nearly resonant light. Changing the parameters of the trapping light like wavelength and intensity not only changes the collisional processes, but also the conditions of the trap itself. Therefore trap loss was studied by inducing collisions with an additional laser beam, the so-called catalysis beam or probe beam, which provided a more direct way of observing the light induced collisions. This lead to the development of the new field of optical collisions.

One of the techniques that has been developed to study ultracold collisions is *photoassociation* of ultracold atoms, where colliding atoms absorb a photon and make a transition to a bound state of the excited diatomic molecule, formed by the two colliding atoms. A pair of colliding ground state atoms is thus *associated* into an excited molecular state by absorption of a *photon*. From photoassociation spectra it has been possible to obtain information on molecular systems, such as high precision molecular binding energies, atomic lifetimes, retardation effects and ground state scattering lengths [1–4]. Examples of how this information is extracted from photoassociation spectra will be given in this paper.

It is instructive at this point to compare this new technique of photoassociation of ultracold atoms with the more traditional fields of molecular spectroscopy and collision physics involving excited state atoms at room temperature. In the case of molecular spectroscopy the resolution is limited by the Doppler effect. At room temperature the velocity of the molecules is typically 1000 m/s and the resolution is of the order of several GHz. Thus the signal is in many cases an average over many rotational and vibrational lines making the interpretation of the spectra cumbersome. In the case of ultracold atoms velocities are as low as 10 cm/s and the resolution is no longer limited by the Doppler effect, but by the finite lifetime of the excited state. Furthermore, due to the small kinetic energy only a few rotational and vibrational lines can be excited, which makes the interpretation of the spectra rather straightforward. In the case of collision physics involving excited state atoms the collision time at room temperature is of the order of 0.1 ns, which is much shorter than the lifetime of the excited state (typically 10 ns). Thus the atoms can be excited at long range and remain in the excited state during the collision. At ultracold temperatures, the collision time becomes of the order of the lifetime of the excited state and is in many cases much shorter, thus the system can no longer be excited at long range, since it will decay before the collision takes place. Thus, the system has to be excited *during* the collision. At this point there is no clear distinction between molecular spectroscopy and collision physics, since the ''spectroscopy'' is performed during the ''collision''. Viewed this way the field of photoassociation inherits many of the features of both collisional physics and molecular spectroscopy, but presents new interesting physics of its own.

The principle of photoassociation spectroscopy is explained schematically in Fig. 1. Although photoassociation spectroscopy has been performed for many alkali-metal atoms and also for some metastable rare gas atoms, we will focus in this review on the Na_2 system. Typically a sample of cold ($\approx$1 mK) atoms is produced by laser cooling and held in a trap. The density of atoms in the trap is large enough to have a significant two-body collision rate between ground state atoms. A so-called probe laser detuned red of the atomic resonance ($3S_{1/2} \rightarrow 3P_{3/2}$ for Na) is focussed on the sample of cold atoms and at a certain laser frequency two slowly colliding atoms absorb a photon to produce an electronically excited, translationally cold molecule in a well-defined rovibrational level. The production rate of cold molecules is monitored as a function of probe laser frequency ν and a signal is observed only if the probe laser frequency is resonant with a transition from the ground state to a singly-excited molecular bound state. Note, that contrary to ''traditional'' molecular spectroscopy the frequency is measured with respect to the dissociation limit, which is well known.

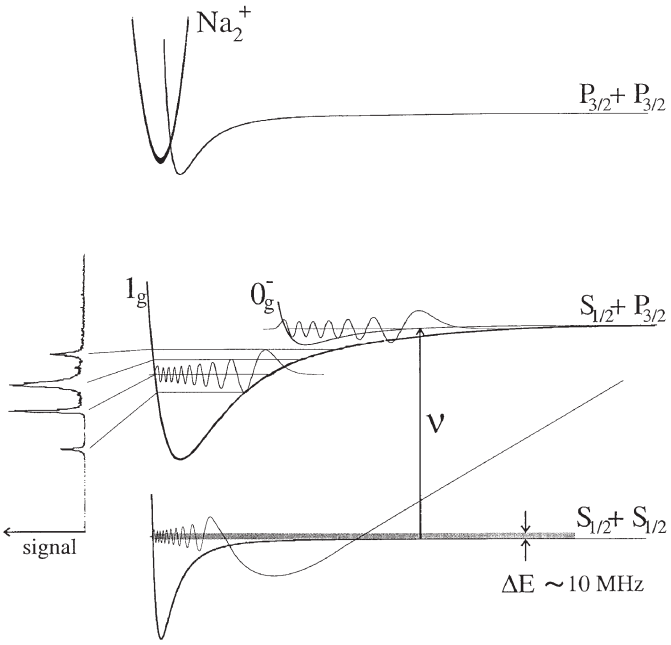

Fig. 1. Schematic diagram showing the ground, excited and doubly-excited state potentials of the Na_2 molecule which are connected asymptotically to the $3S_{1/2}+3S_{1/2}$, $3S_{1/2}+3P_{3/2}$ and $3P_{3/2}+3P_{3/2}$ dissociation limits, respectively. Two atoms colliding slowly in the ground state absorb a red detuned photon to produce an electronically excited, translationally cold molecule in a well-defined rovibrational level. The production rate of cold molecules is monitored as a function of laser frequency ν and the small kinetic energy spread ensures a high resolution.

Since the kinetic energy spread in the atomic sample is very small, the resolution in photoassociation experiments is ≈ 10 MHz (for Na) and thus one or two orders better compared to "traditional" molecular spectroscopy. Moreover, photoassociation spectroscopy has the advantage that it also reveals information about the dynamics of the collisions between slow atoms.

Most of the work on photoassociation has focussed on the alkali-metal atoms. In this comment we will focus on the case of sodium, but recent reviews focussing on potassium [5], rubidium [1] and cesium [6] have been published. Although the principles of photoassociation are identical for all the alkali-metal atoms, the case of Na is special due to the possibility to detect ions produced by absorption of two photons of the photoassociation laser, as will be discussed in Section IB. This not only provides a nearly background free detection method, but also allows for the study of the doubly excited states.

A. *Molecular potentials*

The molecular potentials for alkali-metal dimers are very complex. Especially the molecular potentials at short range ($<30a_0$) display the complicated interactions in the molecular system and reliable potentials can only be obtained by sophisticated quantum chemistry calculations, which have been carried out for the Na_2 system in the group of Masnou and coworkers [7]. However, at long range ($>30a_0$) the interactions are dominated by the electrostatic forces between the valence electrons, which depend on the particular state of the valence electrons. For instance, for atoms interacting at long range in the $S+P$ potential, the long range interaction is fully determined by the dipole–dipole interaction, the interaction potential is given by the C_3/R^3 potential and the long range interaction coefficient C_3 can be calculated from first principles. In the case of the alkali-metals, those coefficients have be calculated by Marinescu and Dalgarno [8,9]. At ultracold temperatures we are only probing the potentials at long range and the analysis of the results can for a large part be carried out without any knowledge of the short range potentials. For the alkali-metal atoms fine structure and even hyperfine structure may play an important role. As was shown by Movre and Pichler [10] for the case of fine structure, those effects can be incorporated in the analysis of the long range dipole–dipole interactions.

In Fig. 2 the potentials connected to the $3S+3P$ asymptote of Na_2 are shown. In Fig. 2a the two asymptotes $3S_{1/2}+3P_{1/2}$ and $3S_{1/2}+3P_{3/2}$ are shown, which are split up by the fine structure splitting in the 3P-state of 515 GHz. In Fig. 2b the region around the $3S_{1/2}+3P_{3/2}$ asymptote is enlarged and one clearly observes the characteristic C_3/R^3 dependence of the potentials combined with the avoided crossings of some of the potentials due to the fine structure interaction. Zooming in more closely on some of the potentials in Fig. 2c,d one observes the splitting of each of those potentials in 10 different potentials, which are split up by the hyperfine interactions. Although the number of states involved becomes large and the detailed shape of the potential becomes complicated, all those features can be calculated relying on a relatively simple model description of the long range forces.

In the experiments discussed in this paper, the probe laser was tuned to the red (blue) of the $3S_{1/2} \rightarrow 3P_{3/2}$ ($3P_{1/2}$) atomic transition frequency. Therefore we only need to consider those molecular potentials which are attractive and asymptotically connecting to the $3S_{1/2}+3P_{3/2}$ dissociation limit. Repulsive potentials connecting to the $3S_{1/2}+3P_{1/2}$ dissociation limit cannot sustain bound states and are therefore of no relevance in the experiments discussed in this paper. Figure 2 shows that five molecular symmetries fulfill the necessary requirements: 1_u, 0_g^-, 2_u, 1_g and 0_u^+. The 1_u potential is a so-called purely long range potential with a well depth of only ≈ 5 GHz, while the 0_g^- potential is also purely long range with a well depth of only ≈ 57 GHz [3,4,11]. These two states, at long range attractive, become repulsive at intermediate internuclear distances of 50–100 a_0 (see Fig. 2b) due to avoided crossings with repulsive states connecting to the $3S_{1/2}+3P_{1/2}$ dissociation limit. Bound levels in these potentials have inner turning points at large internuclear distances and their properties can be calculated to high precision from the atomic properties of Na. The 2_u, 1_g and 0_u^+ potentials remain attractive to much shorter internuclear distances. Transitions from the ground state to the 2_u state are dipole forbidden.

B. *Detection methods*

By monitoring the fluorescence of the trapped atomic sample as a function of probe laser frequency, the photoassociation process can be detected. When a transition is made to a rovibrational level of an attractive molecular state, the atoms are accelerated towards each other, thereby gaining kinetic energy. After spontaneous emission of a photon, the molecule dissociates into two ground state atoms, thereby, according to the Franck–

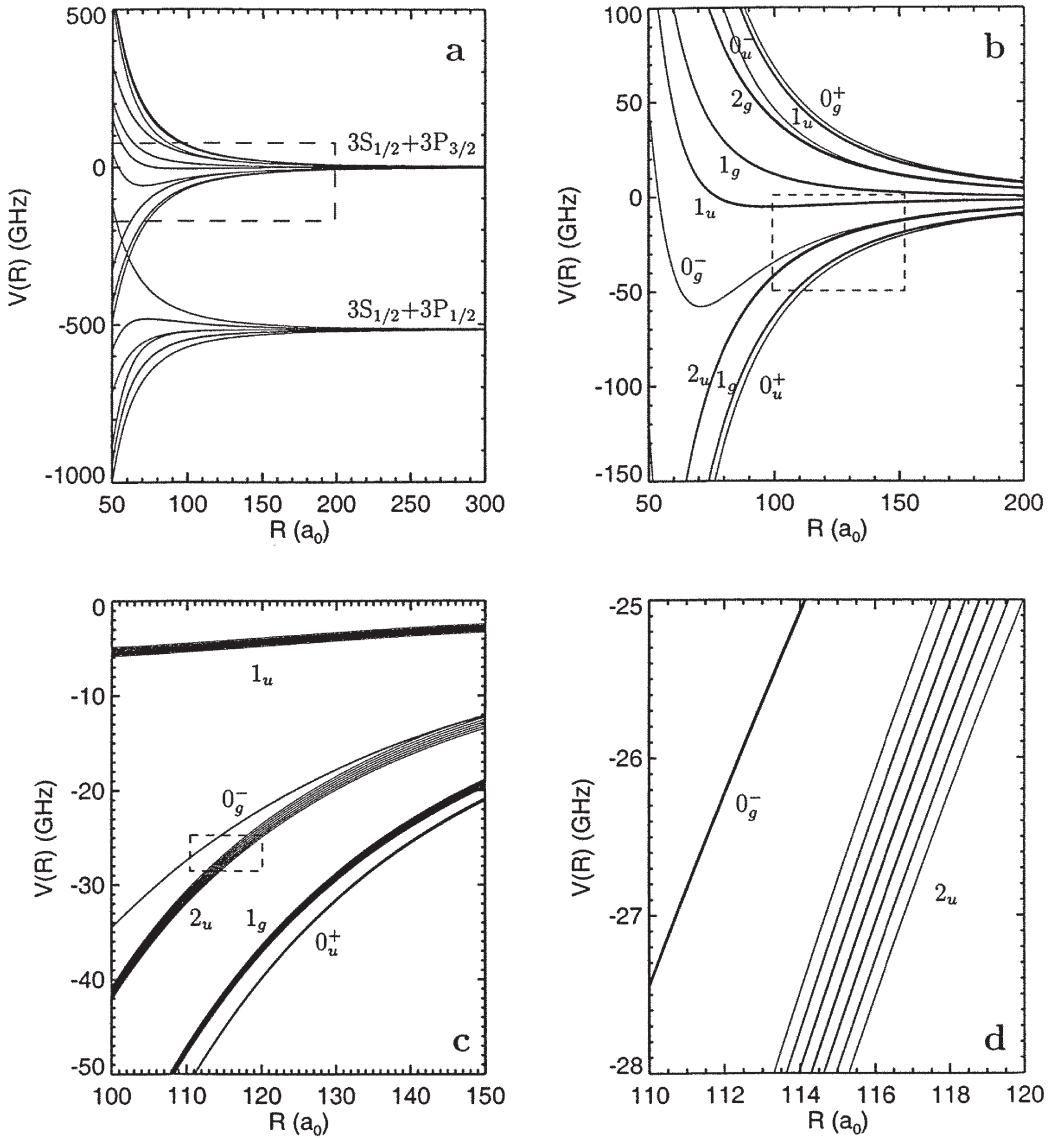

Fig. 2. Calculated Hund's case (c) potential curves for Na_2 connected to the $3S_{1/2} + 3P_{1/2,3/2}$ dissociation limit shown in two different panels. In (a) all the molecular potentials are shown including fine structure (the fine structure splitting is $\Delta_{fs} = 515.52\,\text{GHz}$), (b) shows all the curves connecting to the $3S_{1/2} + 3P_{3/2}$ dissociation limit and (c) shows only the attractive curves connected to this threshold. Finally, in (d) the hyperfine structure of the 2_u state can also be distinguished.

Condon principle, conserving the kinetic energy gained in the excited state (Fig. 3). If the velocity of the atoms gained in the excited state exceeds the capture velocity of the trap v_c, the atoms escape from the trap. This loss from the trap is observed as a decrease in the fluorescence of the trapped atomic sample.

It is also possible to ionize the photoassociated molecules with a second photon of the same frequency and detect the resulting Na_2^+-ions. For Na, there are two pathways leading to ionization: (i) the cold excited molecule is directly photo-ionized at short internuclear distances, which is indicated by photoassociative photoionization (PAPI) in Fig. 3, and (ii) the cold excited molecule is promoted to a doubly-excited state, which autoionizes at short internuclear distances, indicated by photoassociative autoionization (PAAI) in Fig. 3 [12]. If the excitation is in the continuum of the doubly excited states, than the second step adds no structure to the spectrum and the peaks in the ionization spectrum reflects only the structure in the first, photoassociation step.

Since there is no background signal present in the ion spectra, the signal-to-noise ratio for ion spectra is much better than for trap loss spectra [13]. Another disadvantage of the trap loss detection method is that atoms which have not gained sufficient energy in the excited state are not lost from the trap. Excitation to the lowest lying vibrational levels of Na_2^* therefore does not result in an observable trap loss signal. In this paper we will therefore focus on monitoring the photoassociation process by detection of Na_2^+-ions.

II. Results

A. *Single-color photoassociation*

The easiest photoassociation experiment involves one laser to drive both transitions, i.e., the photoassociation and photoionization steps are made with photons of the same frequency ν. Thus we have

$$\text{Na}(3S) + \text{Na}(3S) + h\nu \rightarrow \text{Na}_2^* \tag{1}$$

$$\text{Na}_2^* + h\nu \rightarrow \text{Na}_2^+ + e^- \tag{2}$$

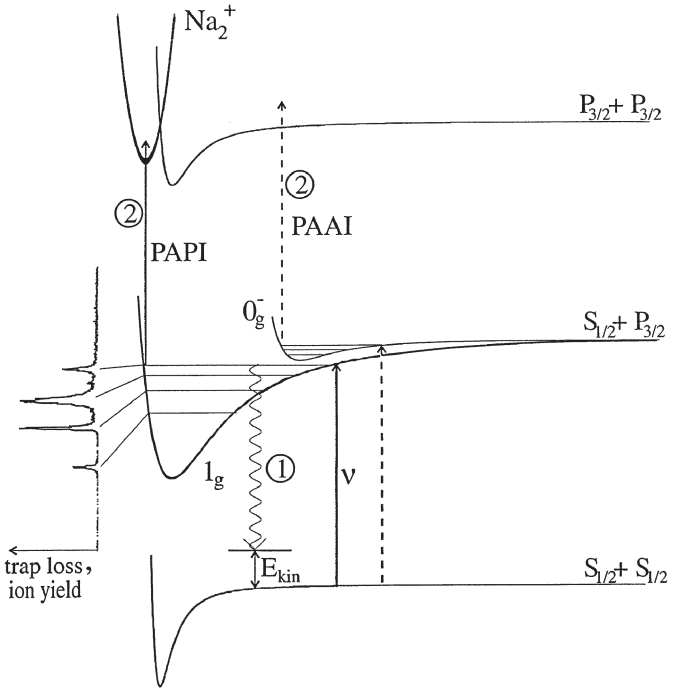

Fig. 3. Schematic diagram showing two ways to detect that a cold molecule is produced. The first method is based on loss of atoms from the trap observable as a decrease of trap fluorescence. In the second method the cold excited molecule is ionized after absorption of a second photon.

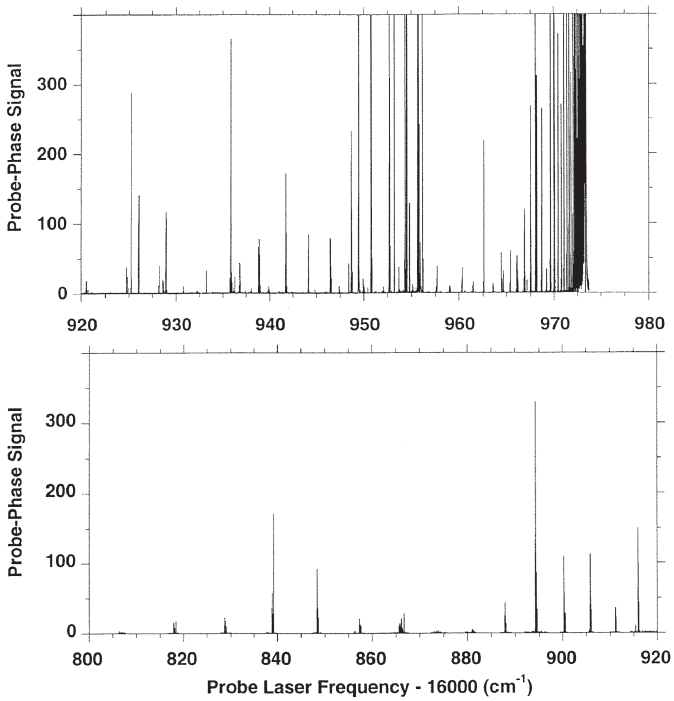

Fig. 4. Single-color photoassociation spectrum showing an ion peak whenever the laser is resonant with a transition from the ground state to a vibrational level of the singly-excited 1_g potential.

where the second step is direct photoionization at short internuclear distances (PAPI). The PAAI mechanism only contributes to the ionization if the total energy of the two photons exceeds the dissociation limit of the doubly-excited states (Ref. [14]). In a single-color experiment this condition is not fulfilled since the frequency of the laser must be tuned to the red of atomic resonance to produce a cold Na_2^*-molecule, and two red detuned photons do not have enough energy to reach the dissociation limit of the doubly-excited states.

A typical single-color photoassociation spectrum is shown in Fig. 4. In the spectrum a typical vibrational structure can be observed, where the spacing between the states becomes smaller close to resonance. Of all the possible singly-excited potentials only the 1_g potential contributes significantly to the spectrum. This is due to the fact that the excitation probabilities for the 0_u^+ and 2_u states are much smaller than for the 1_g state, while the molecules of 0_g^- and 1_u symmetry cannot be ionized using the PAPI mechanism due to their purely long-range character.

B. *Two-color photoassociation*

To be able to study the purely long-range molecules as well, a different ionization mechanism is needed. The long-range molecules can only be ionized using the PAAI mechanism, which requires two laser frequencies. The first laser has to be tuned to the red of atomic resonance for photoassociation to occur and the second laser has to be tuned to the blue of atomic resonance to reach the dissociation limit of the autoionizing doubly-excited states. Instead of using two separate lasers, it is also possible to use one laser and generate a frequency sideband by saturating a single-mode optical fiber [14]. All the incident light above the saturation threshold is completely reflected back and frequency shifted due to Stimulated Brillouin Scattering (SBS) in the fiber. For the fiber used in Ref. [14] the frequency redshift of the backscattered light amounts to $\Delta\nu_{SBS} = 28.5\,\text{GHz}$. A fraction of this SBS light is internally reflected on the entrance facet of the fiber ($R \approx 3.4\%$) and transmitted in the forward direction. Thus at the end of the fiber two frequencies are emerging with a fixed frequency difference of 28.5 GHz. One of these frequencies (ν_{red}) is kept to the red and the other (ν_{blue}) to the blue of atomic resonance. Figure 5 shows the measured ion signal as a function of ν_{red}. The spectrum shows two series of regularly spaced ion peaks. Identification of these peaks is based on their vibrational spacing and hyperfine structure [14–16]. The spectrum in this region is dominated by photoassociation at long range ($R \geq 140\ a_0$) to vibrational levels of the

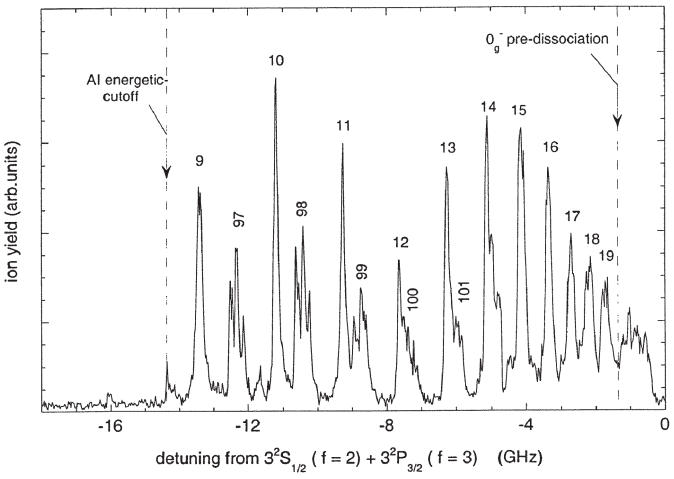

Fig. 5. Measurement of the Na_2^+ signal as a function of ν_{red}. The spectrum shows two series of regularly spaced ion peaks. The series have been identified as the 1_g ($v = 97$–101) and the 0_g^- ($v = 9$–19) vibrational levels. A cutoff of the ion signal is observed at a detuning of $-14.3\,\text{GHz}$.

singly-excited 1_g and 0_g^- potentials, as indicated in the figure.

One thing to be noticed in Fig. 5 is the cutoff of the ion signal at a probe laser detuning of -14.3 GHz, indicated by a dashed line. This cutoff is due to the fact that the frequencies ν_{red} and ν_{blue} are coupled. In the PAAI process only ions are produced if the photon absorbed in the second step has enough energy to promote the molecule to a doubly-excited autoionizing state. Thus the threshold for the PAAI process is given by $\nu_{red} + \nu_{blue} \geq 2\nu_0$ (where ν_0 is the atomic transition frequency). Since $\nu_{red} < \nu_0$ for photoassociation and $\nu_{blue} = \nu_{red} + \Delta\nu_{SBS}$, we find that an ion signal is only observable if the condition

$$\nu_0 - \frac{\Delta\nu_{SBS}}{2} < \nu_{red} < \nu_0 \tag{3}$$

is met. A cutoff of the ion signal is therefore expected at a detuning of 14.26 GHz to the red of the atomic resonance; this is in agreement with the measurements. Note, that such a cutoff would not have been observed if PAPI were the dominant ionization mechanism. The measurement therefore shows that the PAAI process is the dominant ionization mechanism once energetically allowed.

C. *Predissociation*

Another thing to be noticed in Fig. 5 is the sudden disappearance of clearly resolved 0_g^- vibrational peaks for detunings less than 1.5 GHz from atomic resonance. As shown by Stwalley *et al.* the 0_g^- state supports 40 rotationless vibrational states, of which the levels upto state $v = 19$ are clearly resolved. Although the resolution in the experiment is much better than the splitting between the levels, no well-resolved state with $v > 19$ is observed. Instead, the ionization signal is at a minimum at the position of the $v = 20$ state and increases at smaller detunings without any clear vibrational progression.

This behavior can be fully accounted for by carefully examining the detailed potential curves including the fine and hyperfine structure effects. In Fig. 6 we have shown all potential curves with 0_g^- symmetry connected to the $3S_{1/2} + 3P_{3/2}$ asymptote. The inset of that figure shows a detailed look at the curves around -1.5 GHz. There are in total 10 curves with 0_g^- symmetry, which are split up by the hyperfine coupling. For internuclear distances smaller than $300a_0$ all curves seem to connect to the $3S_{1/2}(f = 2) + 3P_{3/2}$ asymptote. However, there is an avoided crossing at $320a_0$ with curves connected to the $3S_{1/2}(f = 1) + 3P_{3/2}$ asymptote and 7 of the 10 curves connect to this asymptote. This crossing is just at the position of the $v = 20$ vibrational state. Thus excitation of this state leads immediately to predissociation of the molecule and does not lead to the formation of molecule in the singly-excited state. This is the reason, why we do not observe ionization of molecules in this state [14]. Note, that although these couplings play a role at very large internuclear distances and are very weak, their effects have a profound influence on the measured spectra.

D. *Vibrational distribution of the ions*

Although these experiments yield detailed information on the dynamics of the process, the final state of the system is not detected. In the last step of the process (see Fig. 3) the system is ionized and the emitted electron can be detected. However, since the electron energies are very small (< 50 meV) this poses experimental difficulty regarding low detection efficiencies, contact potentials and stray magnetic and electric fields. Another technique to obtain information on the final state of the system can be obtained by analyzing the resulting molecular Na_2^+ ions. If we consider the PAAI process, the ions are formed in a crossing between the doubly-excited states and the ionic continuum. Depending on the location of this crossing, ions will be produced in a certain vibrational state and the vibrational state distribution will provide information on the exact location of this crossing, which can be compared to theoretical predictions.

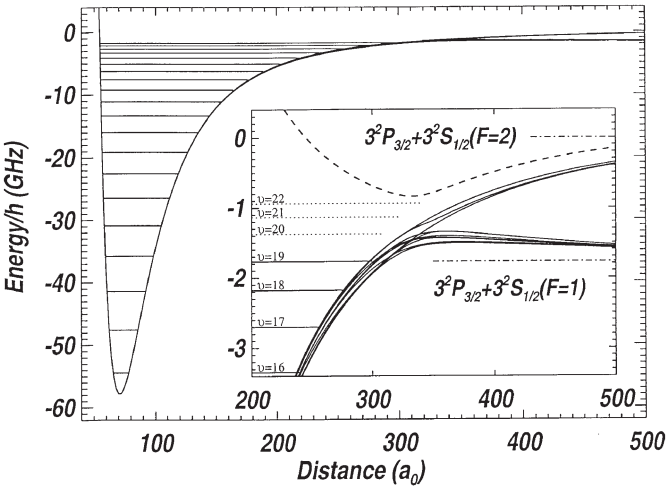

Fig. 6. Calculated potential energies and bound states for the hyperfine components of the 0_g^-. The inset shows an enlarged view for small detunings. The bound states have been indicated with the solid lines. The dotted lines indicate the positions of the hypothetical higher bound states. The dashed line indicates one of the potentials that causes the avoided crossings. Most of the 0_g^- potentials are connected to $3^2S_{1/2}(F_g = 1) + 3^2P_{3/2}$, only three connect to $3^2S_{1/2}(F_g = 2) + 3^2P_{3/2}$.

Blangé *et al.* [12] has measured the vibrational state distribution by photodissociating the formed molecular ions with laser light. The technique relies on the fact, that the overlap between the vibrational state of the ion with a strongly repulsive, higher lying dissociating state will be mainly located at the inner turning point of the dissociation state (see Fig. 7). By scanning the wavelength of the dissociation laser the vibrational state is more or less mapped onto the dissociating state and by detecting the photodissociating rate as a function of the wavelength the vibrational state distribution is reproduced. Note, that the vibrational state distribution depends strongly on the mechanism for the production of the molecular ions. If the PAAI process is responsible for the ion production, then we expect that ions in particular vibrational states to be formed, since that depends on where the crossing takes place. For the PAPI process the vibrational state distribution will be very broad, since the overlap between the intermediate state and the final state does not show any preference for a particular vibrational state.

The results as obtained by Blangé *et al.* [12] are shown in Fig. 8. In the experiment the dissociation cross section shows 4 maxima, which is a clear reflection of the fact that molecular ions are mainly formed in the $v = 3$ state.

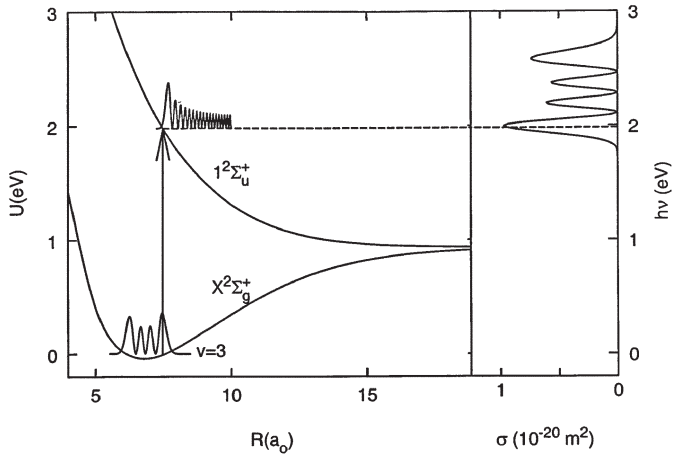

Fig. 7. Schematic diagram of the photodissociation process. Molecular ions formed in a certain vibrational state are photodissociated by excitation to a strongly repulsive state. Since the overlap is located most strongly at the inner turning point of the dissociating state, the vibrational state distribution can be mapped on the wavelength dependence of the dissociation cross section, which is indicated schmatically on the right of the figure.

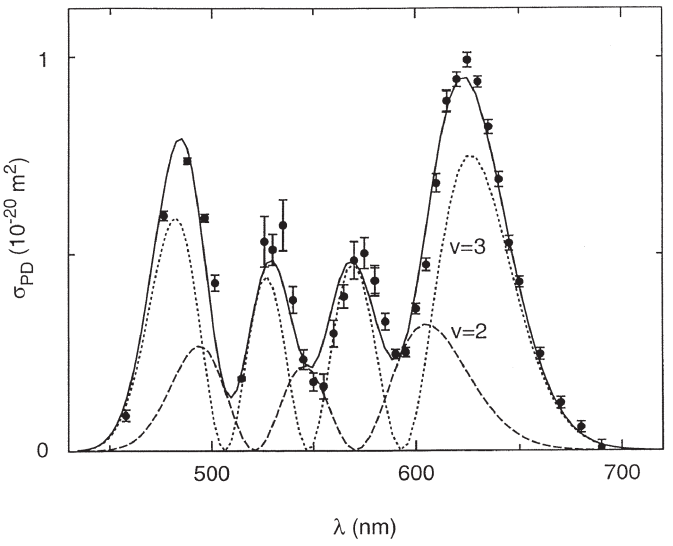

Fig. 8. Measured dissociation spectrum and least-squares fit (solid line) of the experimental data to the calculated spectrum. The dashed lines show the contributions of the various vibrational states to the fit. The error bars on the experimental data represent the statistical uncertainty.

However, since the minima in between the maxima are non-zero, also other vibrational states are populated. Using a theoretical analysis of the photodissociation process the dissociation cross-section for each vibrational state can be calculated. By taking the probability for the production of ions in a vibrational state as a fit parameter, the experimental results can be fitted. The result is shown as a solid line, which fits the experimental results very well. From the analysis one can deduce that the $v = 3$ state is produced with a probability of 70.6%, the $v = 2$ with a probability of 29.1% and the remaining state with less than 1%. The strongly peaked distribution at $v = 3$ is another indication, that the PAAI process is the dominant ionization process for the Na_2^+ ions. The distribution over the $v = 2$ and $v = 3$ state strongly localizes the crossing point between the two curves and this has to be compared with detailed calculations of the potential curves involved.

E. *Spectroscopy of doubly-excited states*

To study the doubly-excited states of Na_2 involved in the PAAI process, the experiment shown schematically in Fig. 9 is performed [17]. The frequency of the so-called photoassociating (PA) laser is fixed to drive a transition from colliding ground state atoms to a specific rovibrational level of the 1_g or 0_g^- potential. The frequency of the second, so-called photoionizing (PI) laser is scanned to drive transitions from the chosen intermediate state to levels up to and above the $3P_{3/2} + 3P_{3/2}$ threshold. By studying the bound states just slightly below this limit the symmetries of the autoionizing doubly-excited states and their properties can be determined. The question of the identity and properties of the autoionizing molecular states connected to the $Na_2(3P + 3P)$ asymptote naturally arises in the study of associative ionization in thermal collisions of Na(3P) atoms as well [18,7,19]. In this case collisions occur on doubly-excited molecular potentials of any symmetry whereas in the case of cold collisions, by choosing the symmetry of the intermediate state, doubly-excited molecular potentials of specific symmetries can be studied separately.

Figure 10 shows a measurement with the PA-laser fixed on the 1_g ($v = 63, J = 1, 2, 3$and 4) states. The bound states are identified as having 1_u and 0_u^- symmetry and from their binding energies it is inferred that the asymptotic potentials are well described by a C_5/R^5 interaction with $C_5 \approx -250$ au for both states. The short range ionization probabilities are determined from the widths of the peaks and it is found that the ionization probabilities are 34% for the 1_u state and 15% for the 0_u^- state. These results provide important tests for quantum chemistry calculations [7,19] which seek to model the

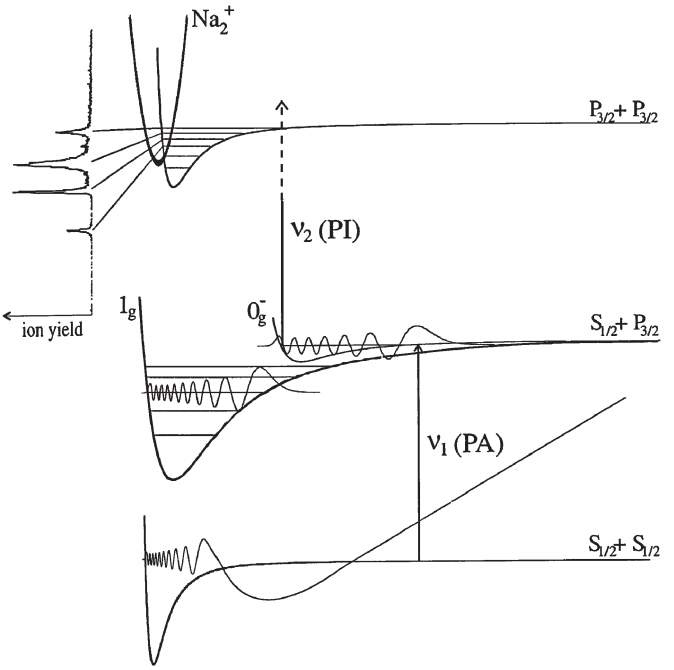

Fig. 9. Schematic diagram of the experiment. The PA-laser (red detuned) is fixed on a rovibrational level of either the singly-excited 1_g or 0_g^- potential (Hund's case (c) notation), while the PI-laser (blue detuned) is scanned through the doubly-excited $P_{3/2} + P_{3/2}$ asymptote. Ion peaks arising below this asymptote are due to excitation of bound doubly-excited states.

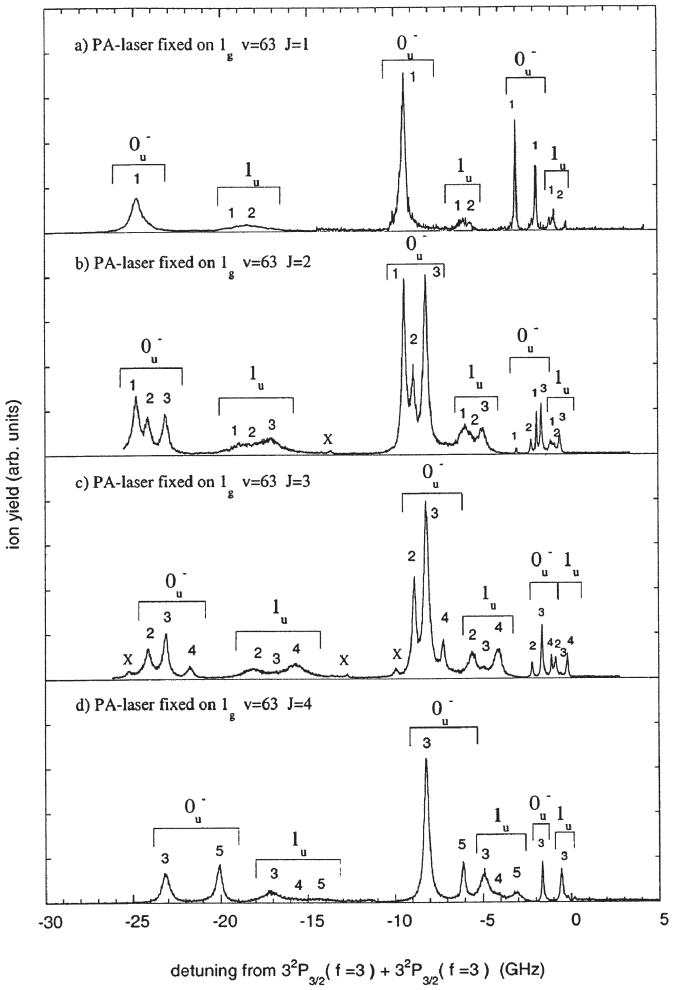

Fig. 10. Measurement with the PA-laser fixed on the 1_g ($v = 63, J = 1, 2, 3$ and 4) states. This vibrational state has an outer turning point at $41\,a_0$. Fixing the PA-laser on different vibrational levels changes the outer turning point and thus the overlap with the doubly-excited states. This is observed as a change in the relative population of the 3 vibrational levels of the 0_u^- and 1_u potentials. The X's indicate unidentified lines, possibly from a 2_u potential.

thermal associative ionization process. Reproducing these results does not require averaging over thermal distributions and molecular symmetries and thus permits a more detailed and direct test of the calculations compared to experiments at thermal energies.

F. *Spectroscopic determination of the scattering length*

It is also possible to determine the ground state *s*-wave scattering length a_s using photoassociation spectroscopy. The scattering length determines the low energy elastic scattering cross section as well as the stability of a Bose–Einstein Condensate and is therefore an important quantity to measure. Figure 11 shows schematically how, in principle, the *s*-wave scattering length can be measured. Given the form of the asymptotic ground state wavefunction,

$$\psi_g(R) \propto \frac{\sin[k(R - a_s)]}{\sqrt{k}} \tag{4}$$

the scattering length a_s is approximately determined by the position of the last node of the ground state wavefunction.

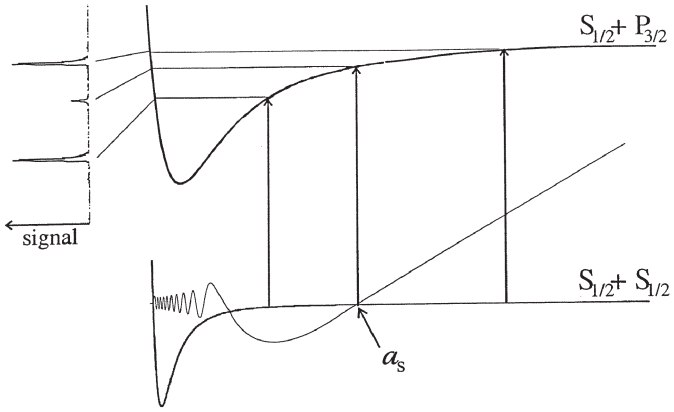

Fig. 11. Schematic diagram explaining how the *s*-wave scattering length may be determined from a photoassociation spectrum.

A node in the ground state wavefunction is reflected in a recorded photoassociation spectrum as a minimum due to the small Franck–Condon wavefunction overlap at the Condon point $R_C = a_s$ (see Fig. 11). Photoassociation spectroscopy has been used to determine the *s*-wave scattering length for Na_2 to $85 \pm 3\ a_0$ [4].

G. *Spectroscopic determination of the atomic Na(3P) lifetime*

The dominant interaction term for the states connecting to the 3S + 3P dissociation limit is the C_3/R^3 dipole–dipole interaction. The value of C_3 is proportional to μ^2 with μ the transition dipole moment $\mu = e\langle 3S|r|3P\rangle$ connecting the 3S and 3P states. The C_3 depends on the relative orientation of the 3S and the 3P atoms, i.e., on the symmetry of the molecular state. It is possible to determine the C_3 coefficient of the purely long range singly-excited 0_g^- potential to great precision by a measurement of the binding energies of vibrational levels in that potential. Using the purely long range 0_g^- state to determine the transition dipole moment μ avoids the uncertainties associated with the potential in the short range chemical-binding region. Since the C_3 coefficient is inversely proportional to the radiative lifetime of the Na(3P) atom, it is possible to measure the atomic Na(3P) lifetime with high accuracy using photoassociation spectroscopy. The result obtained in Ref. [3] of $\tau(3P_{3/2}) = 16.230(16)$ ns helps to remove a longstanding discrepancy between experiment and theory.

III. Conclusion

We have shown that photoassociation spectroscopy is a very powerful technique to determine molecular and atomic properties to great precision. High precision spectroscopy of bound states reveals information about the long range interaction between atoms. In case of the singly-excited Na_2 potentials the long range interaction is given by the C_3/R^3 dipole–dipole interaction. From an accurate measurement of the C_3 coefficient the lifetime of the excited state atom is determined. In case of the doubly-excited Na_2 potentials the long range interaction is given by the C_5/R^5 quadrupole–quadrupole interaction. The C_5 coefficients of two autoionizing doubly-excited states have been determined from photoassociation spectra, as well as

there ionization probabilities. Photoassociation spectroscopy also reveals information about the dynamics of ultracold collisions. The Na_2 *s*-wave ground state scattering length has been determined to great precision using photoassociation spectroscopy. In addition, the ionization pathways have been revealed using a two-color photoassociative ionization technique.

In the future photoassociation spectroscopy will be used to study a variety of other systems. In the case of the alkali-metal atoms there are other long range states in the diatomic molecule, which connect to higher lying asymptotes. These states can be probed using different laser frequencies for the excitation. Since those states will be measured with respect to the dissociation limit and their properties are fully determined by atomic parameters, a detailed comparison between theoretical calculations and experimental results can be made. Photoassociation spectroscopy has also been applied to other systems, like the metastable rare gas atoms. In that case the spectroscopy can not only provide high-resolution results of the molecular potentials, but also yield insight in the dynamics of the Penning ionization process, which is a major loss mechanism for samples of cold, metastable rare gas atoms. Finally, photoassociation can be applied to heteronuclear systems of alkali-metal atoms, for which little information in the literature exists. Those systems are currently being considered as the prime candidates for making a coexisting condensate of two species and information of the interaction potentials is of crucial importance for the behavior of those systems at ultra-cold temperatures.

References

1. Heinzen, D. J., in "Atomic Physics 14," edited by D. Wineland, C. Wieman, and S. Smith (AIP Press, New York), 369 (1995).
2. Lett, P. D., Julienne, P. S. and Phillips, W. D., Annu. Rev. Phys. Chem. **46**, 423 (1995).
3. Jones, K. M., Julienne, P. S., Lett, P. D., Phillips, W. D., Tiesinga, E. and Williams, C. J., Europhys. Lett. **35**, 85 (1996).
4. Tiesinga, E., Williams, C. J., Julienne, P. S., Jones, K. M., Lett, P. D. and Phillips, W. D., J. Res. Natl. Inst. Stand. Technol. **101**, 505 (1996).
5. Stwalley, W. C. and He Wang, J. Mol. Spec. **195**, 154 (1999).
6. Pillet, P., Comm. At. Mol. Phys. ... (2001).
7. Dulieu, O., Magnier, S. and Masnou-Seeuws, F., Z. Phys. D **32**, 229 (1994).
8. Marinescu, M. and Dalgarno, A., Phys. Rev. A **52**, 311 (1995).
9. Marinescu, M., Phys. Rev. A **56**, 4764 (1997).
10. Movre, M. and Pichler, G., J. Phys. B **10**, 2631 (1977).
11. Stwalley, W. C., Uang, Y. and Pichler, G., Phys. Rev. Lett. **41**, 1164 (1978).
12. Blangé, J. J., Zijlstra, J. M., Amelink, A., Urbain, X., Rudolph, H., van der Straten, P., Beijerinck, H. C. W. and Heideman, H. G. M., Phys. Rev. Lett. **78**, 3089 (1997).
13. Jones, K. M., Maleki, S., Ratliff, L. P. and Lett, P. D., J. Phys. B **30**, 289 (1997).
14. Molenaar, P. A., van der Straten, P. and Heideman, H. G. M., Phys. Rev. Lett. **77**, 1460 (1996).
15. Lett, P. D., Helmerson, K., Phillips, W. D., Ratliff, L. P., Rolston, S. L. and Wagshul, M. E., Phys. Rev. Lett. **71**, 2200 (1993).
16. Ratliff, L. P., Wagshul, M. E., Lett, P. D., Rolston, S. L. and Phillips, W. D., J. Chem. Phys. **101**, 2638 (1994).
17. Amelink, A., Jones, K. M., Lett, P. D., van der Straten, P. and Heideman, H. G. M., Phys. Rev. A **61**, 042707 (2000).
18. Weiner, J., Masnou-Seeuws, F. and Giusti-Suzor, A., Adv. At. Mol. Phys. **26**, 209 (1989).
19. Huynh, B., Dulieu, O., Masnou-Seeuws, F., Phys. Rev. A **57**, 958 (1998).

